Two-Dimensional Simulations of CuPc−PCTDA Solar Cells: The Importance of Mobility and Molecular π Stacking

Kristian O. Sylvester-Hvid*

Department of Chemistry, H. C. Ørsted Institute, University of Copenhagen, DK-2100 Copenhagen Ø, Denmark

Received: September 19, 2005; In Final Form: November 21, 2005

An existing two-dimensional microkinetical model for the photovoltaic effect of molecular-based solar cells has been extended to include electron−hole pair recombination between donor and acceptor sites. Simulations of the short circuit current for simple two-dimensional model heterojunction structures composed of copper phthalocyanine (CuPc) and 3,4,9,10-perylenetetracarboxylic dianhydride (PTCDA) are presented. The short circuit current was investigated as a function of the thickness of the photoactive layer for different choices of mobility for CuPc and PTCDA. The hole mobility of CuPc and/or the electron mobility of PTCDA limits the photovoltaic performance if chosen below a certain threshold determined by the net electron−hole generation rate at the CuPc−PTCDA interface. Also, the mobilities should be of the same order of magnitude. The effect of changing the interplanar separation α between the π stacking molecules was investigated, and it was found that increasing α from 0.33 to 0.6 nm increases the short circuit current up to 5 orders of magnitude. This was rationalized in terms of the charge separation energetics of geminate electron−hole pairs and its dependence on α. As mobilities decrease with increasing α and thus opposes this effect, an optimum for $\alpha \sim 0.66$ nm was found for the CuPc−PTCDA heterojunction model structures. The simulations are interpreted in a simple kinetic picture of an electron−hole pair generation step at the CuPc−PTCDA interface and subsequent transport in the CuPc and PTCDA domains. It is argued that an optimal device configuration involves an amorphous region at the CuPc−PTCDA interface and a gradual increase of the molecular order as the electrodes are approached in the respective CuPc and PTCDA transport regions.

Introduction

Since the first perylene/metal phthalocyanine based photovoltaic (PV) devices,[1] a vast number of studies have been devoted to improving their PV efficiency using different derivatives of perylenes and metal phthalocyanines incorporated into various device structures.[2] However, only little progress has been achieved in terms of improving the efficiency of these solar cells, the highest efficiency reported so far of 2%[3] being clearly too low for practical solar cell applications. Accordingly, within the past decade or two focus has shifted from the perylene/metal phthalocyanine based solar cells to the more efficient polymer−fullerene based solar cells.[4] Despite their better efficiencies and processability, the photoactive polymer−fullerene films however still lack the required robustness for outdoor/long-term solar cell applications, properties that are more likely to be achieved with perylene and metal phthalocyanine derivatives.

In this theoretical study, focus is specifically on the model compounds 3,4,9,10-perylenetetracarboxylic dianhydride (PTCDA) and copper phthalocyanine (CuPc) and their incorporation into thin-film heterojunction PV devices as n- and p-type molecular semiconductors,[40] respectively. Under illumination or the locus of an energy transfer process, CuPc and PTCDA may act as a donor−acceptor couple and give rise to an intermolecular charge transfer (CT) reaction. This provides the increase in chemical potential as required for separation of unscreened, Coulomb-bound electron−hole pairs ($e^- - h^+$) in a molecular based (low-dielectric) PV device.

CuPc and PTCDA are strongly absorbing (optical absorption lengths in the range of 50−100 nm) and widely available blue and red dyes, respectively, and combined either by sequential deposition or codeposition in device films cover a substantial part of the visible solar spectrum.[2] CuPc and PTCDA show extraordinary chemical and photophysical stability; they neither bleach nor are degraded by the ambient surroundings. Contrary to the polymer−fullerene PV devices, where the presence of oxygen is devastating, for CuPc oxygen in fact acts as a dopant without which CuPc would become isolating, and the corresponding CuPc/PTCDA PV device ceases to work.[3] Being highly symmetric and planar π-conjugated molecules, they feature attractive structural packing properties in the condensed phases: in the crystalline phases molecular packing involves π stacking with interplaner separations[5] as small as 0.3 nm in a certain direction (exceptionally small for van der Waals bound materials) which explains the relatively high mobilities observed for both crystalline PTCDA and CuPc (10^{-4} $m^2/(V\ s)$ for CuPc single crystals[6]). In the amorphous phases characteristic of vapor-deposited thin films, the degree of molecular π stacking largely depends on the deposition conditions, cold substrates favoring more amorphous morphologies with less spatial order.

The above properties make CuPc and PTCDA (and their derivatives) viable candidates for optoelectronic devices as such, and a vast number of studies seeking to characterize structural, optical, and electrical properties of their thin films have been conducted over the past decades. In particular, thin films of PTCDA have been investigated in great detail by a variety of

* Present address: Freiburger Materialforschungzentrum, Stefan-Meier-Strasse, 21, D-79104 Freiburg i. Br., Germany. Web: www.sylvesterhvid.dk/kristian.

10.1021/jp055321h CCC: $33.50
Published on Web 01/25/2006

experimental techniques, the results of which provide a solid understanding of the electrical and photophysical properties of PTCDA.[5]

From a technological point of view, the disadvantage of CuPc and PTCDA is the necessity of vacuum deposition in the fabrication of devices, and in practice derivatization is required to allow solution-based, large-scale processing of thin-film PV devices. However, from a simulation point of view, CuPc and PTCDA are interesting as generic and representative structures for the wider class of soluble derivatives—i.e., simple and well-defined device structures can be made with CuPc and PTCDA and input for simulations can be extracted from the extensive literature on CuPc and PTCDA thin films.

Despite extensive investigations and a deep understanding of both CuPc and PTCDA thin films on many types of substrates, the efficiency of CuPc/PTCDA PV devices has not improved significantly.[3,7−10] Factors limiting the efficiency are the low charge mobilities μ and short exciton diffusion lengths d_{ex} characteristic of the amorphous films. The former leads to large series resistance on increasing device thickness to the point were substantial incident light is absorbed, and the latter limits the volume of the photoactive film that actually contributes to the photocurrent.[2]

For perylene/ZnPc PV devices it has been argued that the active charge generating region in fact is limited to within ∼5 nm of the heterojunction interface.[11] Also the purity and hence the lack of unintentional recombination/dissociation centers seem to be important.

To improve efficiencies there are consequently two ways to proceed: increase μ and d_{ex} by imposing ultrahigh purity and as-close-to crystalline molecular order in the films, thus allowing for increased device thickness,[5] or employ very thin amorphous CuPc/PTCDA bilayers (reducing resistance and making all excitons reach the DA interface) folded in space by means of nanopatterned electrode structures or interpenetrating device structures (to ensure sufficient light absorption).

Here the effect of changing the degree of molecular order is investigated for thin CuPc/PTCDA bilayers by means of simulations.

Optimization and the understanding of the CuPc/PTCDA PV device performance is addressed by means of simple two-dimensional (2D) microkinetic simulations conducted for microscopic model structures with device thicknesses of up to 60 nm, as schematically shown in Figure 1. The thickness dependence is an essential experimental device parameter, the tuning of which ultimately requires a thorough understanding of both macro- and microscopic processes in the PV device.

The simulation model employed is an extension of the model used previously to study the dependence of the short circuit current (I_{sc}) on the blend morphology of polymer−fullerene based solar cells.[12,13] Being microscopic, the model treats a representative subvolume of the photoactive thin film and provides a detailed kinetic description of the steady-state charge carrier dynamics of the illuminated 2D volume. The extension as presented here amounts to the inclusion of a recombination pathway into the existing manifold of electron transfer (ET) pathways defining the dynamics of the PV system. For the CuPc/PTCDA heterojunction devices as illustrated in Figure 1 (henceforth referenced as CuPc|PTCDA), such simulations are particularly feasible due to the simple morphology and can therefore be performed for small representative (narrow) structures.

From mobility studies of single carrier (electron or hole) organic thin-film devices, it is generally recognized that the mobility is closely related to the degree of molecular order. Much experimental effort has therefore been devoted to achieving long-range (mesoscopic) order in organic thin films, e.g., by employing perylene or phthalocyanine derivatives with their tendency to form π stacks. However, the implicit assumption of structural order and close packing as being also, *and always*, beneficial for the PV performance is challenged in this study from the point of view of the charge separation (CS) dynamics of photogenerated electrons and holes. In simulating I_{sc}, emphasis will therefore be on the importance of structural order/disorder of the thin films, using a simple and qualitative picture for the degree of spatial disorder of the CuPc and PTCDA molecules.

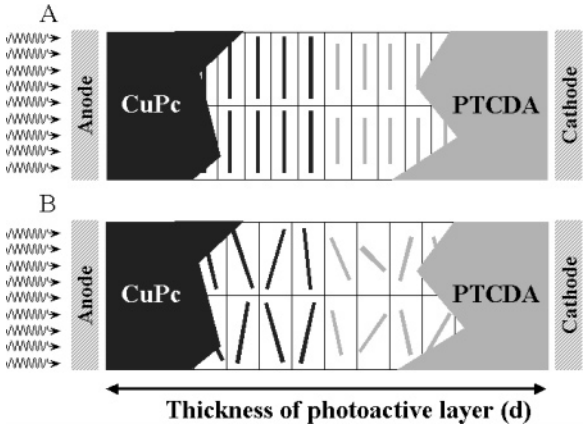

Figure 1. Schematic illustration of the microscopic two-dimensional CuPc|PTCDA heterojunction devices investigated by simulations. The bars on the grid represent planar CuPc (dark gray) and PTCDA (light gray) molecules as viewed from the side along the molecular plane. In (A) the molecules are arranged in closed-packed coplanar π stacks whereas in (B) orientational disorder has been introduced to mimic a more amorphous phase.

Taking the CuPc|PTCDA system as a generic model for PV devices based on planar π stacking donor and acceptor molecules, from the simulation results it is argued that too much structural order in the vicinity of the donor−acceptor interface in fact limits the PV performance. The results suggest therefore a more nuanced view on such heterojunction solar cells, namely, that the photoactive film should be amorphous in the vicinity of the donor−acceptor interface and gradually turn more ordered toward the electrode interfaces.

The Model

The microkinetic PV model approximates the thin-film PV device with a 2D grid of illuminated donor (D) and acceptor (A) sites positioned between (virtual) electrodes as sketched in Figure 1. Each site contains either a donor (dark gray) or an acceptor (light gray) molecule, both shown with bars in Figure 1. Hence, the dark gray region constitutes the p-type phase and the light gray region the n-type phase, the overall device being then a molecular-based pn-junction illuminated through the anode. The thickness of the PV model system in Figure 1 corresponds here to the thickness of the photoactive molecular film of the real device, here designated *d*, and typically spans a range of 50−100 nm. The transversal dimension (normal to light incidence) of the system in Figure 1, here also referred to as its width, is limited to two or three sites in this study. By virtue of the pseudo-one-dimensional character of the heterojunctions considered, I_{sc} scales linearly with the number of sites in the transverse direction and no additional information is gained on increasing the width, but from the gradual elimination

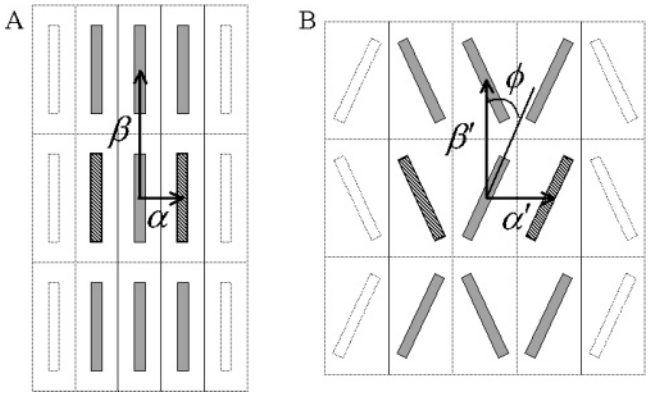

Figure 2. Illustration of the nearest neighbor interaction region in a (A) well-ordered coplaner arrangement and (B) orientationally disordered arrangement of the molecules in the PV device. α and β designate respectively the longitudinal and transversal molecular center-of-mass separations or the length and width of the grid sites. In (B) ϕ designates the average angular displacement away from the well-ordered coplanar arrangement of the molecules as in (A).

boundary effects. The simulations yield, therefore, *microscopic* values of I_{sc} which, for the questions addressed in this study, contain sufficient information to be conclusive.

As D and A correspond, respectively, to the planar CuPc and PTCDA molecules, the dark and light gray bars in Figure 1 simply represent these molecules as viewed from the side along their molecular planes. Figure 1A illustrates a situation with a high degree of order, the molecules forming coplanar crystalline π stacking arrangements. Conversely, Figure 1B illustrates a situation where some *orientational* disorder has been introduced. The two situations in Figure 1 refer therefore to the approximations made when simulating either highly ordered or more amorphous CuPc|PTCDA thin-film PV devices.

The photoinduced charge carrier dynamics is described by *nearest neighbor* hopping of an electron and a hole among the molecular sites on the grid shown in Figure 1. In Figure 2 the nearest neighbor hopping region for a given site is shown for the general case, with the eight nearest neighbor sites highlighted in gray and black. The longitudinal center-of-mass (CM) separation between the molecules is α and the transversal separation β, corresponding also to the length and width, respectively, of the grid unit employed in the simulations. Parts A and B of Figure 2 correspond to the ordered and orientationally disordered situations in parts A and B of Figure 1, respectively. On introducing disorder, α increases to α′ and β decreases to β' and thus gives rise to an average molecular angular displacement (tilt angle) of ϕ.

Approximating spatial disorder of amorphous molecular films by orientational disorder alone, as illustrated in Figures 1 and 2, indeed is a simplified picture of the structural changes occurring with the transition from the crystalline to the amorphous phase. The approximation does however capture the essential feature with a minimum of structural parameters (α and β), namely, that the interplanar distance between disk-shaped molecules on average is expected to increases as the phase becomes amorphous.

To illustrate the photoinduced charge carrier dynamics in greater detail, consider the simple one-dimensional DD|AA system shown in Figure 3. Donor (dark gray) and acceptor (light gray) sites (the molecules) are represented in terms of their HOMO and LUMO levels[41] and the anode and cathode in terms of ejection and injection levels. Each site may occupy from one to three electrons (not shown) and thus can be either of the following species; X, X*, X^+, and X^-, where X designates either

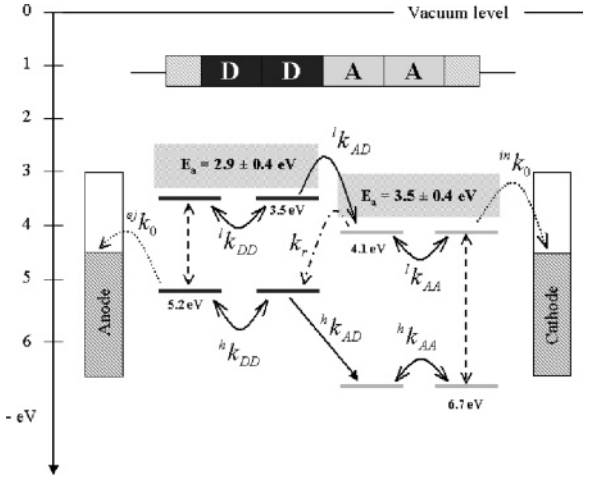

Figure 3. Schematic illustration for a simple one-dimensional DD|AA system of all the possible electron-transfer path ways as accounted for by the microkinetic PV simulations. Each arrow corresponds to two rates: a generic for the downhill transition as shown and a Boltzmann weighted rate for the uphill transition. Donor (dark gray) and acceptor (light gray) sites are represented in terms of their HOMO and LUMO levels and the anode and cathode in terms of ejection and injection levels. Also shown are the energetic position of the electron affinity for the donor and acceptor materials.

D or A. Shown also in Figure 3 are the energetic positions of the electron affinity for the donor (E_a^D) and acceptor (E_a^A) materials. The possible ET pathways included in the model are shown by arrows in Figure 3: filled arrows indicate either D ↔ D, A ↔ A, and D → A transitions via HOMO or via LUMO levels. Dotted arrows indicate the ejection/injection of electrons into the cathode/anode, required to occur such that the system maintains overall charge neutrality. The broken-dotted arrow designates the newly implemented recombination pathway between a LUMO level on an A site and the HOMO level on a neighboring D site. Finally, broken arrows indicate the vertical optical transitions on the D and A sites. Each arrow in Figure 3 corresponds to two rates: a generic rate, k, for the downhill transition (as shown) and a Boltzmann weighted rate $k' = k \exp(-\Delta E_{ij}/k_b T)$ for the uphill transition (not shown). The device temperature is T, and ΔE_{ij} is the energy difference between states i and j of the system as connected by the ET process. Apart from the recombination process, the dynamics of the model has been described previously[12,13] and only recombination is addressed below.

Charge recombination eliminates a nearest neighbor (geminate) $e^- - h^+$ pair and corresponds to state transitions characterized by the process $\cdots D^+ - A^- \cdots \rightarrow \cdots D - A \cdots$, which here is an exothermic process. Note that (⋯) designates the rest of the PV system which is unchanged by the transition. The simulations account only for a single geminate $e^- - h^+$ pair in the system, and for this case any recombination process will take the state of the PV system to its ground state, i.e., the state with all neutral and nonexcited D and A molecules. With the ground state energy arbitrarily set to zero, all states characterized by the $\cdots D^+ - A^- \cdots$ configuration are given the energy E_{DA}^{ct}. Accordingly, the rate for the *reverse* recombination process ($\cdots D - A \cdots \rightarrow \cdots D^+ \text{-} A^- \cdots$) then is $k_r^r = k_r \exp(-\Delta E_{DA}^{ct}/k_b T)$.

Generally nearest neighbor $e^- - h^+$ pairs occur in the following situations: at DA interfaces ($\cdots D^+ - A^- \cdots$ and $\cdots A^+ - D^- \cdots$), within the D phase ($\cdots D^+ - D^- \cdots$), and within the A phase ($\cdots A^+ - A^- \cdots$). States of the PV system characterized by such configurations are here referred to as charge-transfer states (ct-states) and are assigned the energies: E_{DA}^{ct}, E_{AD}^{ct}, E_{DD}^{ct}, and

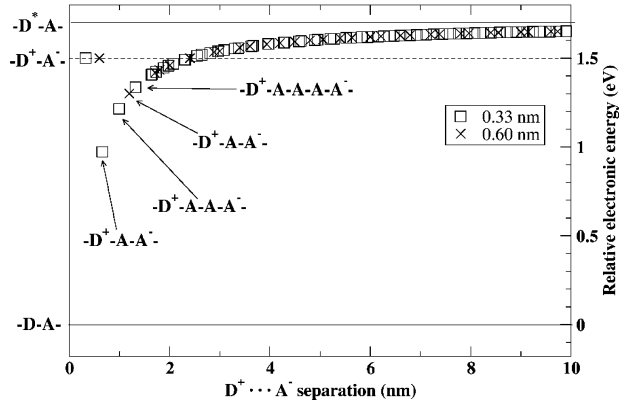

Figure 4. Electrostatic energy for $\cdots D^+ \cdots A^- \cdots$ configurations versus the geminate $e^- - h^+$ pair separation R for heterojunction structures with $\beta = 1.6$ nm and $\alpha = 0.33$ nm (□) or $\alpha = 0.6$ nm (×).

E_{AA}^{ct}, respectively. The ct-states are nearest neighbor cases of the general charge-separated states (cs-states), the configurations of which are represented as $\cdots X^+ \cdots Y^- \cdots$, where the electron and hole are separated by distance R and the state energy approximated as[13,14]

$$E_{XY}^{cs}(R) = I_p^X - E_a^Y - \frac{e^2}{4\pi\chi R} \quad (1)$$

In eq 1 I_p^X and E_a^Y are the ionization potential of material X = {D,A} and electron affinity of material Y = {D,A}, respectively. The third term in eq 1 describes the Coulomb potential due to point charges localized at the cationic (X^+) and anionic (Y^-) sites, separated by R within a dielectric medium of average dielectric constant χ. Note that eq 1 assumes no built-in field (vide infra). Figure 4 shows the electrostatic energy derived from eq 1 with $\alpha = 0.33$ or 0.6 nm and $R \leq 10$ nm, for PV system states characterized by the configurations $\cdots D^+ \cdots A^- \cdots$. It may be inferred that the point-charge approximation of eq 1 is problematic for highly π-conjugated molecules as addressed here, but at least for PTCDA it has been shown[15] that the $e^- - h^+$ pair interaction follows a point-charge-like Coulomb potential for all but the nearest neighbor separations (the ct-states). In the latter case the energy is derived by other means, and from Figure 4 clearly is much larger than that otherwise obtained with eq 1.

The interaction energy of $e^- - h^+$ pairs for the other three types of configurations ($\cdots A^+ \cdots D^- \cdots$, $\cdots D^+ \cdots D^- \cdots$, and $\cdots A^+ \cdots A^- \cdots$) all have the same Coulombic shape as the $\cdots D^+ \cdots A^- \cdots$ interaction potential shown in Figure 4, but are shifted upward in energy due to other values of I_p^X and E_a^Y in eq 1. As expected for a PV system driven largely by the chemical potential gradient across the DA interface, the energetics of the photoinduced $e^- - h^+$ pair primarily is determined by the $\cdots D^+ \cdots A^- \cdots$ potential, for which reason the other potential curves are not shown in Figure 4.

As seen from Figure 2 one should distinguish between sitewise and distancewise nearest neighbors in those cases where α and β are very different. Hence, if $2\alpha < \beta$, then *next* nearest neighbors 2α away may in fact be closer than nearest site neighbors β away in the other direction. Here the sitewise notion is used to determine the possible nearest neighbor couplings. However, for the energy of states characterized by $\cdots D^+ - A^- \cdot \cdot$ configurations, only nearest neighbor configurations with site separation α have a non-Coulombic energy E_{DA}^{ct}. These neighboring sites are shown with black bars in Figure 2.

The distance dependence of the nearest neighbor couplings (the ET rates) is approximated with

$$k(R) = k_0 \exp(-\gamma[R - R_0]) \quad (2)$$

where γ is the electronic coupling decay factor for the particular ET process and R_0 the reference distance at which the rate is given as input for the simulation. The assumption here is that electronic coupling between molecules occurs from CM to CM.

In the simplified picture of the charge carrier dynamics adopted here, only nearest neighbor *single particle* hopping events are included. Exciton migration (diffusion) can therefore not be described as this involves moving two electrons simultaneously—although a small secondary contribution to exciton migration can occur through two-step processes.[42] As exciton migration largely is neglected by the model, only those excitons located right at the DA interface contribute to charge generation. The model is therefore biased in terms of its sensitivity toward DA interface features, and with respect to the total number of excitons generated (none of which can migrate), the model will underestimate the I_{sc}.

As indicated in Figure 3 the HOMO and LUMO levels of both D and A occur at identical energies throughout the device structure. This being the general picture, the model employs the so-called flat-band condition, a situation normally only attained at an external bias corresponding to the built-in potential, V_{in}. Here V_{in} is neglected all together and flat-band conditions are assumed when the PV system is operated under short circuit conditions. By adoption of this approximation, the additional driving force facilitating CS and which is due to V_{in} is disregarded and the model is further biased toward underestimating I_{sc}.

The incident solar radiation is approximated by a Planckian blackbody radiation distribution characterized by the radiation temperature T_{rad}. The radiation absorption/emission occurs only at the two frequencies corresponding to the HOMO−LUMO transition of D and A, respectively. This indeed is a major approximation but simplifies the photogeneration dynamics to a point where the only important parameter is T_{rad}. In fact, I_{sc} shows a strong dependence on T_{rad} (related to the intensity), and by tuning T_{rad} it is possible to calibrate I_{sc} to correct for misrepresentations of the solar irradiance distribution or other shortcomings of the model—if so desired.

Further, a constant radiation intensity throughout the photoactive film is assumed which, as shown in several studies, is not correct due to frequency-dependent interference phenomena in the layered thin-film structures.[19]

Simulation Details

Rates for the nearest neighbor ET processes are extracted from experimental or theoretical sources where available and otherwise rely on qualified guessing. For hopping among similar sites ET rates are derived from the corresponding electronic mobility of the pure materials, i.e., the zero-field electron (μ_e) and hole mobilities (μ_h) for CuPc and PTCDA. Writing the diffusion coefficient as $D = kl^2$ and the mobility in terms of the Einstein relation, $\mu = De/k_bT$,[28] an average microscopic ET rate may be approximated as

$$k = \frac{\mu k_b T}{el^2} \quad (3)$$

valid at low internal field strengths. In eq 3 l refers to a mean hopping distance for the particular ET process and is taken as

TABLE 1: Various Parameters As Used in the CuPc|PTCDA Simulations

quantity	significance
$l_{DD} = 0.34$ nm	smallest interplanar distance in CuPc[3]
$l_{AA} = 0.32$ nm	smallest interplanar distance in PTCDA[3]
$\alpha = 0.33$ nm	length of grid units[16]
$\beta = 1.60$ nm	width of grid units[16]
$R_0 = 0.33$ nm	ref distance in eq 2
$\gamma_{diss} = 10.4$ nm^{-1}	$^1/_5$ of decay factor for exciton dissociation from ref 17
$\gamma_{rec} = 13.0$ nm^{-1}	$^1/_5$ of decay factor for recombination from ref 17
$\gamma_0 = 10.0$ nm^{-1}	default decay factor (assumption)
$\epsilon = 3.0$	average static dielectric constant
$T = 300$ K	device temperature
$T_{rad} = 1300$ K	radiation temperature[18]

TABLE 2: ET Rates As Employed in the CuPc|PTCDA Simulations

ET process	rates (s^{-1})	basis
$D^H \rightarrow D^H$	${}^hk_{DD} = 10^{10}$	eq 3, $l_{DD} = 0.34$ nm (ref 3) and $\mu_h \sim 10^{-7}$ m^2/(V s)[20,21]
$D^L \rightarrow D^L$	${}^lk_{DD} = 10^8$	eq 3, $\mu_e \sim 10^{-9}$ m^2/(V s)[a,22−24] and $l_{DD} = 0.34$ nm (ref 3)
$A^H \rightarrow A^H$	${}^hk_{AA} = 10^{11}$	eq 3, $l_{AA} = 0.32$ nm (ref 3) and $\mu_h \sim 10^{-6}$ m^2/(V s)[27]
$A^L \rightarrow A^L$	${}^lk_{AA} = 10^8$	eq 3, $l_{AA} = 0.32$ nm (ref 3) and $\mu_e \sim 10^{-9}$ m^2/(V s)[27]
$D^L \rightarrow A^L$	${}^lk_{DA} = 10^{14}$	see text
$D^H \rightarrow A^H$	${}^hk^{DA} = 10^3$	assumption
$A^L \rightarrow D^H$	$k_r = 10^2$	see text
$A^L \rightarrow$ cathode	${}^{in}k_0 = 10^{10}$	assumption
anode $\rightarrow D^H$	${}^{in}k_0 = 10^{10}$	assumption

[a] Reported μ_e varies between 10^{-10} and 10^{-8} m^2/(V s).

TABLE 3: Energy Parameters for CuPc and PTCDA As Employed in the CuPc|PTCDA Simulations

quantity	CuPc (eV)	PTCDA (eV)
I_p	5.2[30,31]	6.7[31]
E_{opt}	1.7[14,32]	2.6[14,33]
E_t	2.3 ± 0.4[14]	3.2 ± 0.4[14]
E_{ct}	1.9	2.3

the smallest interplaner separation in CuPc and PTCDA, respectively (see Table 1). The mobilities used to derive ET rates generally are those of amorphous films as deposited at ambient temperature and are listed in Table 2.

Unless specifically stated, the reference distance R_0 used in eq 2 is an average of l_{DD} and l_{AA} and the electronic coupling decay factor γ_0 taken as 10 nm^{-1} [43] as also listed in Table 1.

The essential ET processes between D and A sites are exciton dissociation with rate ${}^lk_{AD}$ and recombination with rate k_r, both shown in Figure 3. In a theoretical study by Lemaur et al.,[17] ${}^lk_{AD}$ and k_r were estimated to 3.6×10^{13} s^{-1} and 1.7×10^2 s^{-1}, respectively, for a coplanar arrangement of the Pc−PTCDI dimer (in the gas phase) at separation 0.4 nm. The corresponding electronic coupling decay factors obtained there were $\gamma_{diss} = 52$ nm^{-1} and $\gamma_{rec} = 65$ nm^{-1}. As seen from Table 1, here these values have been corrected by a factor of 1/5 to qualitatively account for the effect of the surrounding medium in the condensed phase.[29] Using these values of γ_{diss} and γ_{rec} in eq 2, ${}^lk_{AD}$ and k_r at $R_0 = 0.33$ nm are approximated with 10^{14} s^{-1} and 10^2 s^{-1}, respectively.

The energy parameters required by the simulations are summarized in Figure 3 and Table 3. The positions of the HOMO levels in Figure 3 are approximated by the ionization potentials given in Table 3, and the LUMO levels are given as $I_p - E_{opt}$, where E_{opt} is the absorption maximum of the $S_1 \leftarrow S_0$ transition.[44] The electron affinity, E_a, as shown with uncertainties in Figure 3, is taken as $I_p - E_t$, where E_t is the electrical transport gap for the material. Hence, within this simplified picture $(I_X^p - E_X^a) - E_{opt}^X$ is the exciton binding energy in material X, and from Table 3 it amounts to 0.6 ± 0.4 eV for both CuPc and PTCDA. That the Frenkel excitons are bound is also clear from Figure 3 displaying all LUMO levels below the electron affinities.

Apart from I_p, E_a, and E_{opt}, the required parameters for the energy model are the energies for the ct-states. For the D and A materials, E_{DD}^{ct} and E_{AA}^{ct} are estimated from the CT absorption bands found just above and below the $S_1 \leftarrow S_0$ absorption peak for CuPc and PTCDA films, respectively. Hence for CuPc, the $\cdots D^+-D^-\cdots$ type states are found 0.1−0.2 eV higher in energy than $\cdots D^*-D\cdots$ type states[34] and E_{DD}^{ct} is taken as $E_{opt}^D + 0.2$ eV $= 1.9$ eV. Conversely, for PTCDA the $\cdots A^+-A^-\cdots$ type states are found at 0.2−0.3 eV lower energy than $\cdots A^*-A\cdots$ type states,[5,25,35,36] and $E_{AA}^{ct} = E_{opt}^A - 0.3$ eV $= 2.3$ eV. E_{DA}^{ct} is estimated from the calculated energy difference between the D*−A and D^+-A^- states for the coplanar arrangement of the Pc−PTCDI dimer at separation 0.4 nm,[17] and therefore $E_{DA}^{ct} = E_{opt}^D - 0.2$ eV $= 1.5$ eV. The value of E_{AD}^{ct} has been addressed neither experimentally nor theoretically but certainly should be larger than E_{opt}^A. It is assumed that $\cdots A^+-D^-\cdots$ configurations are 0.5 eV higher in energy than $\cdots A^*-D\cdots$ configurations and therefore that $E_{AD}^{ct} = E_{opt}^A + 0.5$ eV $= 3.1$ eV.

The observed 0.4 eV vacuum level displacement for CuPc|PTCDA heterojunction structures[31] is disregarded altogether as also evident from Figure 3.

Simulation Results

First the effect on I_{sc} of explicitly changing the mobility is investigated. Although the mobility generally is linked to the level of molecular disorder, changes in mobility here are done at a constant level of disorder, i.e., at constant molecular separation ($\alpha = 0.6$ nm and $\beta = 1.6$ nm). Subsequently, the effect of molecular disorder on I_{sc} is explicitly investigated. For a given simulation, I_{sc} is generally derived for thicknesses (d) of the photoactive layer ranging from the thickness of a single DA bilayer and up to 60 nm. In the following such a data series is discussed under one heading and referenced as $I_{sc}(d)$.

Mobility Dependence. It is interesting to identify the isolated contribution to $I_{sc}(d)$ resulting from changing the mobility of a single component under PV conditions. This is done by performing simulations for fictitious PV structures referred to as pureA and pureD and shown as inserts in Figure 5. These structures are heterojunctions with either the D (pureA) or the A (pureD) phase removed to the point where only the charge generating DA interface remains, which then resides directly at the anode or the cathode, respectively. The pureA simulations do not depend on the CuPc mobilities, μ_e^D and μ_h^D, and in Figure 5A $I_{sc}(d)$ is shown as derived for different orders of magnitude of the PTCDA mobilities μ_e^A and μ_h^A. These are varied over ±3 orders of magnitude relative to the reference values listed in Table 2. $I_{sc}(d)$ simulated for the reference values of μ_e^A and μ_h^A is displayed with (◇) and dashed lines in Figure 5A. Similarly, for the pureD simulations which do not depend on μ_e^A and μ_h^A, results for $I_{sc}(d)$ derived for ±3 orders of magnitude of μ_e^D and μ_{sh}^D are shown in Figure 5B, and the reference mobility results again are shown with (◇) and dashed lines.

From Figure 5 I_{sc} is seen to decline with increasing thickness of either the PTCDA or CuPc layer. Consequently, for each monolayer of PTCDA or CuPc added to the DA bilayer, a

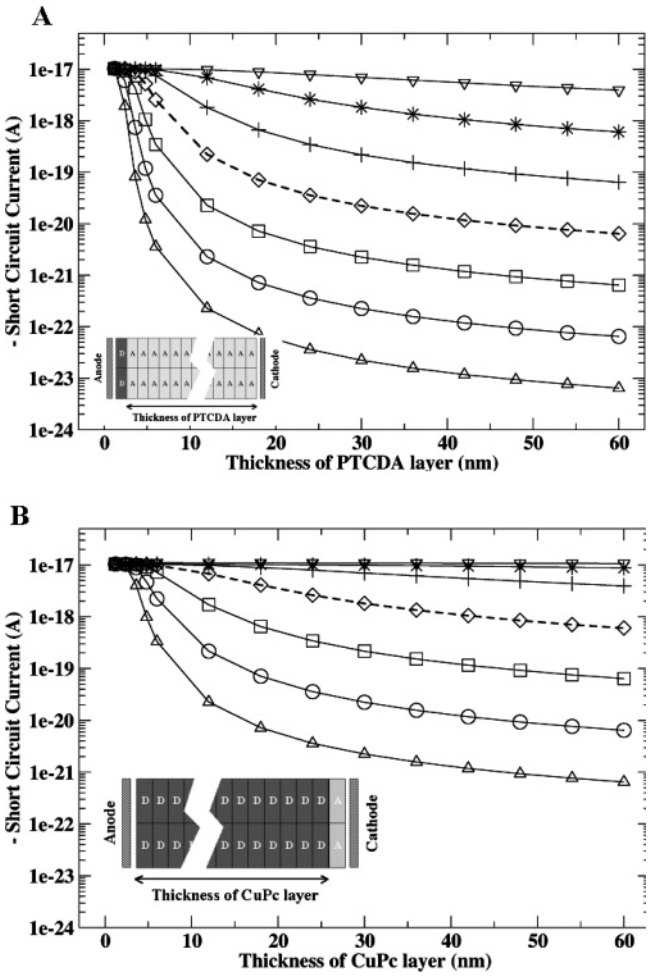

Figure 5. $-I_{sc}$ versus layer thickness for (A) "pure" PTCDA devices using reference mobilities (◇) $\mu_e^A = 10^{-9}$m^2/(V s) and $\mu_h^A = 10^{-6}$m^2/(V s) and (B) "pure" CuPc devices using reference mobilities (◇) $\mu_e^D = 10^{-9}$m^2/(V s) and $\mu_h^D = 10^{-7}$m^2/(V s). Results obtained with the corresponding mobilities multiplied by 10^{-3} (△), 10^{-2} (○), 10^{-1} (□), 10 (+), 10^2 (∗), and 10^3 (▽) are also shown. Results are derived using $\alpha = 0.6$ nm and $\beta = 1.6$ nm.

decrease in the PV performance results in accord with the model assumption of no exciton diffusion.[45] Hence, increasing the PTCDA (pureA) or the CuPc (pureD) layer thickness only increases the series resistance, the effect being most pronounced for the pureA structures as seen on comparing $I_{sc}(d)$ in parts A and B of Figure 5.

For layer thicknesses greater than ~20 nm, increasing either the PTCDA (pureA) or CuPc (pureD) mobilities an order of magnitude implies ca. a corresponding order of magnitude increase in $I_{sc}(d)$, as seen from Figure 5. However, from Figure 5B it is clear that on increasing μ_e^D and μ_h^D more than a factor 10 relative to the reference mobilities, the increase in $I_{sc}(d)$ ceases for the pureD structures.

To assess the importance of the hole mobility in the PTCDA phase, and the importance of the electron mobility in the CuPc phase, simulations similar to those leading to Figure 5 were conducted, but changing only μ_e^A and μ_h^D for the pureA and pureD structures, respectively. On the log scale employed in Figure 5 these results (as omitted here) appear identical to Figure 5. This implies that the ambipolar nature of PTCDA and CuPc can be neglected here and that the pureA and pureD results can be analyzed exclusively in terms of μ_e^A and μ_h^D, respectively.

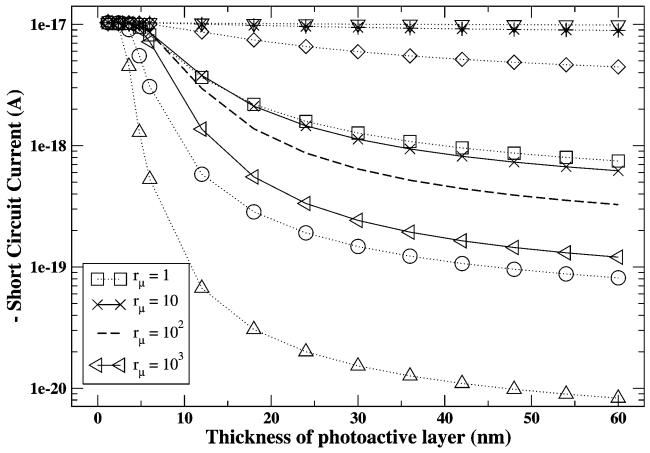

Figure 6. $-I_{sc}$ versus layer thickness d for CuPc|PTCDA structures simulated for different choices of μ_h^D and μ_e^A. With dotted lines are displayed results obtained for $\mu_h^D = \mu_e^A$: 10^{-10} (△), 10^{-9} (○), 10^{-8} (□), 10^{-7} (◇), 10^{-6} (∗), and 10^{-5} m^2/(V s) (▽). Also shown are results obtained for a mobility mismatch r_μ of 10 (×, solid line), 100 (dashed line) and 1000 (left open triangle, solid line) which should be compared to the $\mu_h^D = \mu_e^A = 10^{-8}$ m^2/(V s) (□) result. Results are derived using $\alpha = 0.6$ nm and $\beta = 1.6$ nm.

From Figure 5B it may be inferred that increasing μ_h^D above 10^{-6} m^2/(V s) leads to no further increase in PV performance for the corresponding CuPc|PTCDA heterojunction. Conversely, from Figure 5A, μ_e^A may be increased at least by 3 orders of magnitude with the PV performance still improving. To affirm these conclusions, simulations similar in terms of changing μ_h^D and μ_e^A were conducted, but for CuPc|PTCDA structures (see insert in Figure 7) with d up to 60 nm. Although displaced with respect to the magnitude of I_{sc}, these results (as omitted here) show similar trends as those in Figure 5, namely, a general decline of I_{sc} with increasing d and an order of magnitude increase in $I_{sc}(d)$ as μ_h^D or μ_e^A increases a corresponding order of magnitude. However, the saturation of $I_{sc}(d)$ occurs already at $\mu_h^D \sim 10^{-7}$ m^2/(V s) for the CuPc|PTCDA structures, and not at $\mu_h^D \sim 10^{-6}$ m^2/(V s) as for pureD in Figure 5B.

The fact that on increasing mobilities, $I_{sc}(d)$ saturates for μ_h^D and not for μ_e^A, combined with the reference value of μ_h^D being 2 orders of magnitude larger than for μ_e^A, indicates that balancing the mobilities is important for device performance. This is in contrast with simulation results due to Peumans et al.,[37] suggesting that a mobility mismatch $r_\mu = \mu_h^D/\mu_e^A$ of up to 3 orders of magnitude should improve the PV performance for molecular disordered heterojunction devices. To address this discrepancy, simulations of $I_{sc}(d)$ for CuPc|PTCDA structures were conducted varying $\mu_h^D = \mu_e^A$ over 6 orders of magnitude, the results of which are shown with dotted lines in Figure 6. Clearly, increasing $\mu_h^D = \mu_e^A$ from 10^{-7} to 10^{-6} m^2/(V s) leads to saturation of $I_{sc}(d)$ in a fashion similar to what is seen in Figure 5B. This suggests that by increasing μ_e^A 2 orders of magnitude (balancing μ_h^D and μ_e^A), the series resistance in the PTCDA layer is reduced to a point where the $e^- - h^+$ pair generation at the DA interface becomes the limiting kinetic step. Also shown in Figure 6 with solid and dashed lines are $I_{sc}(d)$ as simulated for $r_\mu = 10^n$ and $n = \{1, 2, 3\}$, invoked with a symmetric increase and decrease of μ_h^D and μ_e^A, respectively. The $r_\mu = 10^2$ curve (no symbols) corresponds to $I_{sc}(d)$ as derived for the reference values of μ_h^D and μ_e^A in Table 2. The effect of the mobility mismatch should be compared to the $\mu_h^D = \mu_e^A = 10^{-8}$ m^2/(V s) (□) result ($r_\mu = 1$), and clearly increasing r_μ hampers the PV performance as seen from Figure 6.

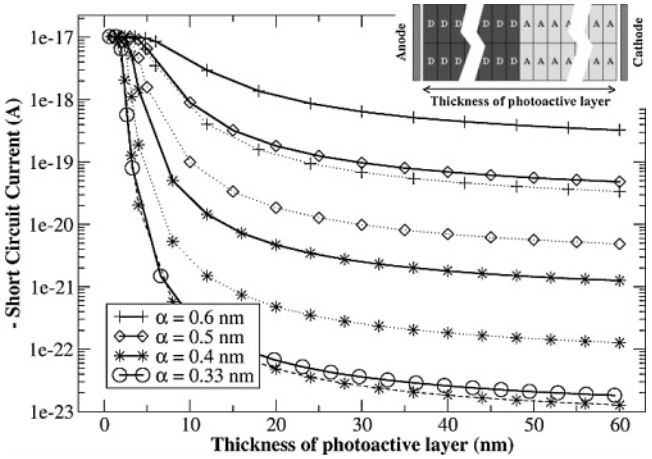

Figure 7. $-I_{sc}$ versus the thickness of the of the photoactive layer for CuPc|PTCDA heterojunction structures as simulated using $\beta = 1.6$ nm and α equal to 0.33 nm (○), 0.4 nm (∗), 0.5 nm (◇), and 0.6 nm (+). Also shown are selected results obtained by multiplying $\mu_{e,h}^{A}$ and $\mu_{e,h}^{D}$ with 0.1 (dotted lines) and 0.01 (dashed lines).

Effect of Disorder. With $\gamma = 10$ nm^{-1}, according to eq 2 an order of magnitude decrease in the ET rate may result if the coupling (hopping) distance increases by ∼0.2 nm, and likewise for the mobility according to eq 3. By the interdependence between mobility and I_{sc} as seen from Figure 5 and by eq 3, one should thus expect a 0.2 nm increase in α to decrease $I_{sc}(d)$ approximately by an order of magnitude. To test this, $I_{sc}(d)$ was simulated for CuPc|PTCDA structures using $\beta = 1.6$ nm and α = {0.33, 0.40, 0.50, and 0.60 nm} for different choices of mobilities, the results of which are shown in Figure 7. Looking first at $I_{sc}(d)$ obtained for the reference mobilities (shown with solid lines), the opposite and quite dramatic effect is observed: $I_{sc}(d)$ increases roughly *2 orders of magnitude* for each 0.1 nm increase in α, and on increasing α from 0.5 to 0.6 nm, by 1 order of magnitude. Hence, despite that mobilities as such decrease with increasing α, a significant increase in PV performance is seen on increasing α up to 0.6 nm. To quantify this effect in terms of changing the mobilities, the α = 0.40, 0.50, and 0.60 nm simulations were repeated employing now $\{\mu_h^A, \mu_e^A\}$ and $\{\mu_h^D, \mu_e^D\}$ multiplied by 0.1 (dotted lines). Additionally, for α = 0.40 nm simulations using $\{\mu_h^A, \mu_e^A\}$ and $\{\mu_h^D, \mu_e^D\}$ multiplied by 0.01 (* and dashed line) were done. As seen from Figure 7, it takes a 2 orders of magnitude decrease in all mobilities to compensate for the increase in $I_{sc}(d)$ as α is increased from 0.33 to 0.4 nm. Increasing α from 0.4 to 0.5 nm and from 0.5 to 0.6 nm, it takes an order of magnitude mobility increase to counteract the increase in $I_{sc}(d)$. The overall result of Figure 7 is clear: increasing α by ∼0.3 nm increases $I_{sc}(d)$ by 4 to 5 orders of magnitude.

Obviously, the increase of $I_{sc}(d)$ with α must cease after some optimum is reached, and to find this, simulations of I_{sc} for CuPc|PTCDA structures either 40 sites or 100 site long were conducted for α ranging between 0.33 and 0.90 nm. In Figure 8 results are shown for I_{sc} versus α derived for CuPc|PTCDA structures 100 sites long. To investigate the extent to which the optimum of $I_{sc}(\alpha)$ depends on the energy of the ···D$^+$···A$^-$··· ct-states, the simulations were performed for the range of E_{DA}^{ct} values shown in Figure 8. As seen, on increasing E_{DA}^{ct} up to 1.5 eV the magnitude of $I_{sc}(\alpha)$ increases accordingly and the optimum moves toward larger α. From $E_{DA}^{ct} = 1.4$ eV and up to 1.8 eV, $I_{sc}(\alpha)$ is virtually unaffected with $\alpha_{opt} \sim 0.66$ nm.

The corresponding results obtained for structures only 40 sites long (not shown here) are qualitatively similar to those in Figure 8 and also yield an optimum for $I_{sc}(\alpha)$ at $\alpha_{opt} \sim 0.66$ nm. Further, simulations similar to those leading to Figure 8 were performed but changing E_{AD}^{ct}, E_{DD}^{ct}, and E_{AA}^{ct}. They showed that $I_{sc}(\alpha)$ is unaffected by changing these energy parameters (results are omitted here) which points to that I_{sc} is governed primarily by the CS and recombination dynamics on the ···D$^+$···A$^-$··· potential energy curve shown in Figure 4.

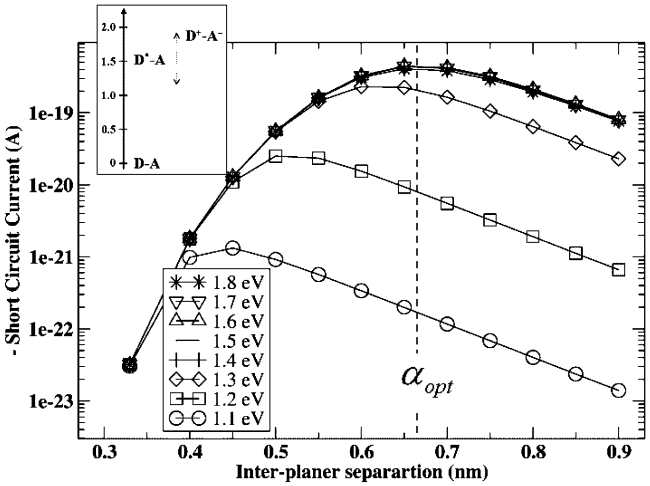

Figure 8. $-I_{sc}$ versus the intermolecular stacking distance α as simulated for CuPc|PTCDA structures 100 sites long using different choices of E_{DA}^{ct}.

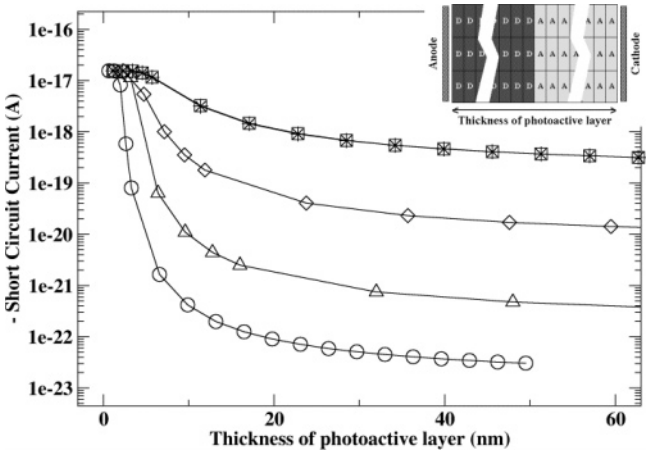

Figure 9. $-I_{sc}$ versus the thickness of the photoactive layer of CuPc|PTCDA heterojunctions three sites wide as simulated for average tilt angles ϕ of 10° (□), 45° (◇), and 90° (△). Also shown are the coplanar cases where $\beta = 1.6$ nm and α = 0.33 nm (○) or α = 0.57 nm (∗).

Molecular spatial disorder is represented as orientational disorder and quantified by the average molecular tilt angle ϕ as shown in Figure 2. To investigate the effect of disorder within this picture, in Figure 9 results for $I_{sc}(d)$ simulated for CuPc|PTCDA structures, now three sites wide and using ϕ = {10°, 45°, and 90°} are shown.[46] As seen, orientational disorder corresponding to an average tilt angle of 10° (α = 0.57 nm and $\beta = 1.57$ nm, shown with □) enhances $I_{sc}(d)$ up to 4 orders of magnitude relative to the coplaner α = 0.33 nm situation (shown with ○). For ϕ equal to 45° (◇) and 90° (△), $I_{sc}(d)$ decreases with about 1 and 2 orders of magnitude, respectively, relative to the $\phi = 10°$ situation. The $\phi = 90°$ case corresponds to the situation where α and β have been interchanged and where the $E_{DA}^{ct} = 1.5$ eV correction now applies for the transversal nearest neighbors a distance α away. For $\phi = 45°$, the E_{DA}^{ct} =

1.5 eV correction applies for nearest neighbors in both directions because $\alpha = \beta$.

To compare the effect of representing orientational disorder through simultaneous adjustments of both α and β with that of increasing α only, results for $I_{sc}(d)$ simulated for $\alpha = 0.57$ nm and $\beta = 1.60$ nm are also shown in Figure 9. Clearly, the effect of imposing an average tilt angle of 10° on $I_{sc}(d)$ can equally well be represented by changing α only, i.e., the effect of changing β from 1.60 to 1.57 nm is insignificant. The results shown in Figure 9 were all obtained from simulations on PV structures three sites wide to ensure that at least some sites (the middle ones) had a full nearest neighbor coupling region.

Discussion

All simulations where μ_e^A and/or μ_h^D were changed show that the lower the mobility is, the larger is the increase in the series resistance with the thickness of the photoactive layer. For molecular-based heterojunctions, where increasing the layer thickness beyond the exciton diffusion length only adds series resistance,[2] this result is important: it shows that I_{sc} may drop several orders of magnitude within the first 10−20 nm, in case the mobility is chosen too low. Another general result is that for thicknesses larger than ~20 nm, the effect of increasing μ_e^A and/or μ_h^D an order of magnitude is a corresponding order of magnitude increase in I_{sc}. This occurs irrespective of the structures considered, but only as long as the transport process corresponding to the mobility considered is kinetically limiting. That $I_{sc}(d)$ saturates on increasing μ_h^D above some threshold means that the hole transport in the p-type region no longer constitutes a bottleneck. Increasing μ_h^D further leaves $I_{sc}(d)$ unchanged as the net e^-−h^+ generation rate at the DA interface then becomes kinetically limiting.

Although not physically realizable, the pureA and pureD (collectively referred to as pure{A,D}) structures are considered because they offer a convenient way to assess, independently, the importance of the mobility of only one component under operational PV conditions. Pure{A,D} simulations allow thus a unique determination of the magnitude of μ_e^A and μ_h^D, respectively, at which n- and p-type charge transport becomes kinetically limiting for a system with a given net e^-−h^+ generation rate at the DA interface. For example, changing μ_h^D over 6 orders of magnitude (at fixed μ_e^A) for CuPc|PTCDA structures showed that increasing μ_h^D beyond 10^{-7} $m^2/(V\ s)$ does not increase the PV performance further. However, for the pureD simulations (Figure 5B) where there is no limiting (resistive) contribution from a PTCDA layer, the results show in fact that μ_h^D must be increased beyond 10^{-6} $m^2/(V\ s)$ for hole transport not to be limiting. This could of course also have been arrived at considering CuPc|PTCDA structures but would have required more simulations, probably scanning the entire (μ_e^A, μ_h^D) parameter space. Pure{A,D} simulations offer the direct route and moreover quantify to what extent the individual CuPc and PTCDA monolayers contribute to the PV performance. Here I_{sc} is consistently largest for the thinnest pure{A,D} structures and always falls off with increasing d. As this is also the case for the heterojunctions considered, the results suggest a simple picture of the CuPc|PTCDA structures as consisting effectively of a charge generating DA bilayer embedded between p- and n-type transport regions. The general decline of I_{sc} with increasing thickness of the photoactive layer seen for all simulations is in contrast to experimental observations (and simulations) for related molecular PV devices.[2] The discrepancy can primarily be attributed to the neglect of exciton diffusion in the simulations. Had it been included then the charge generating interface region would have had a characteristic thickness of d_{ex} and $I_{sc}(d)$ been increasing for d below ~d_{ex}.

For the p- and n-type transport regions, the results show that the mobility for the respective majority carriers must be balanced not to compromise the PV performance, in direct contradiction with the suggestions by Peumans et al.[37] In particular, the results in Figure 6 underscore that a mobility mismatch ($r_\mu = 10^3$) larger than constituted by the reference values of μ_h^D and μ_e^A ($r_\mu = 10^2$), does *not* improve $I_{sc}(d)$, rather it is lowered. The discrepancy between this result and the findings of Peumans et al.[37] could be due to their assumption of all steps following initial e^-−h^+ pair separation, to be 100% efficient ($\eta_{CT}\cdot\eta_{CC} = 1$). By this assumption, the kinetic and coupled nature of the system is neglected, and with this the fact that the transport regions may slow the net charge generation rates for unbalanced and/or low values of μ_e^A and μ_h^D.

That $I_{sc}(d)$ in Figure 5 is not affected by changing the mobilities of the minority carriers (μ_h^A and/or μ_e^D) for the n- and p-type regions indicates that for heterojunction devices, the ambipolar nature of CuPc and PTCDA is without significance. Hence, the p- and n-type nomenclature used throughout is justified. However, this might well be different for bulk heterojunctions with fine-grained morphologies or other structures with a high degree of D and A mixing.

The results in Figure 7 indicate that for molecular PV devices employing tight packing of planar molecules, the PV performance is governed by the CS energetics of the short e^-−h^+ pairs. That increasing α (thus decreasing coupling rates for longitudinally connected neighboring sites) in fact increases $I_{sc}(d)$ by orders of magnitude at first seems counterintuitive. However, Figure 4 suggests that for $\alpha = 0.33$ nm trapping of ···D^+···A^-··· configurations (with small e^-−h^+ separation) in the potential well is more likely than when $\alpha = 0.60$ nm. Note that the potentials in Figure 4, by virtue of the energetic ··· D^+−A^-··· configurations (ct-states), are not simple Coulomb potentials leading e^-−h^+ pairs directly into recombination. The assumption of nearest neighbor hopping implies that in the course of e^-−h^+ pair separation, the state of the PV system must pass through the ···D^+−A^-···, ···D^+−A−A^-···, and ··· D^+−A−A−A^-··· configurations, among others. For small α, in particular the ···D^+−A−A^-··· and ···D^+−A−A−A^-··· configurations[47] represent rather trapped e^-−h^+ pairs, as also evidenced by the higher degree of charge polarization of the DA interface under such conditions (D side being positive and A side negative).

The likelihood of escaping these trapping configurations increases with α as they then move out of the deep part of the potential well—compare, e.g., the potentials in Figure 4. As a result, interface polarization which blocks e^-−h^+ pair generation is diminished thus improving the PV performance. Hence, it is primarily stabilization of short e^-−h^+ pairs at the DA interface which for small α impedes the PV performance, rather than a relative increase in recombination with decreasing D−A separation, the latter because γ_{diss} and γ_{rec} are of similar magnitude.

For α smaller than $\alpha_{opt} = 0.66$ nm, the lowering of $I_{sc}(d)$ with decreasing α by no means is compensated by the corresponding increase in the mobilities for the transport regions; as established it takes at least an order of magnitude increase in mobilities to compensate the decrease in $I_{sc}(d)$ caused by a 0.1 nm decrease in α. For α larger than $\alpha_{opt} = 0.66$ nm, the trapping of short e^-−h^+ pairs becomes less pronounced, but then the exponential decrease of mobilities with increasing α (through eq 2) sets in, hence increasing the device series

resistance. $\alpha_{opt} = 0.66$ nm constitutes a compromise between these opposing effects for the CuPc|PTCDA structures investigated. Note that the determination of α_{opt} is merely of conceptual importance here, as the actual number will critically depend on the order/disorder model employed.

For consistency, the energy of all $\cdots D^+-A^-\cdots$ type states, E_{DA}^{ct}, was approximated not to depend on α. Thus, for simulations where α was changed, the driving force for $\cdots D^*-A\cdots \rightarrow \cdots D^+-A^-\cdots$ remained constant.[48] This approximation is born out of necessity because $E_{DA}^{ct}(\alpha)$ is unknown and eventually should be assessed quantum chemically. However, from Figure 8 it is established that $I_{sc}(\alpha)$ is unaffected by changing E_{DA}^{ct} between 1.4 and 1.8 eV, and within this interval attains the largest values. Conversely, for $E_{DA}^{ct} < 1.4$ eV does $I_{sc}(\alpha)$ depend on E_{DA}^{ct} and in such a way that, if E_{DA}^{ct} would decrease with α, then $I_{sc}(\alpha)$ would decrease more drastically with α than in Figure 8.

The results in Figure 9 indicate that a modest level of orientational disorder ($\phi = 10°$) may substantially improve PV performance, an effect which wears off as more disorder is introduced however ($\phi = 45°$ and 90°). The pseudo-one-dimensional character of the CuPc|PTCDA heterojunction is emphasized by the fact that the $\phi = 10°$ (□) result can equally well be obtained with $\alpha = 0.57$ nm and $\beta = 1.60$ nm (*). To this end it should be kept in mind that the spatial 2D representation of the CuPc and PTCDA phases, ordered as well as disordered, obviously implies gross simplifications and that the results therefore merely express an expected trend. E.g., the microscopic picture employed of molecular disorder does not correspond to the experimental reality where the amorphous phase is composed of a distribution of nanocrystallites.[20,38,39]

Conclusion

Extension of a 2D microkinetic PV simulation tool to include e^--h^+ recombination has been described and simulations performed for simple CuPc|PTCDA structures. They showed that I_{sc} may qualitatively be rationalized within a simple kinetic picture of an optically pumped e^--h^+ pair generation step and subsequent transport steps. The different kinetic steps of the system are intimately coupled, and appropriate matching of rates is required to obtain good PV efficiency.

In particular, the matching of rates is relevant for the hole and electron transport in the p- and n-type regions, respectively, which translates into numerical matching of μ_e^A and μ_h^D. It was shown that as long as electron and/or hole transport is kinetically limiting, a 10-fold increase in mobility results in a 10-fold increase in I_{sc}.

Using a primitive structural model for the π stacking of the CuPc and PTCDA molecules, it was shown that the PV performance is very sensitive to the choice of α. Increasing α from 0.33 nm to 0.6 nm improved $I_{sc}(d)$ by 4 to 5 orders of magnitude, the underlying reason being less trapping of short e^--h^+ pairs at the DA interface. Opposing this effect is the general decline in both mobilities and coupling rates across the D−A interface with increasing α. For the CuPc|PTCDA structures investigated, an optimal interplaner separation was estimated to 0.66 nm.

By use of an increase in α (and decrease in β) to mimic orientational molecular disorder, it was shown that an average angular molecular displacement of 10° relative to the molecular planes in the corresponding ordered structures improves the PV performance significantly. This indicates that some amorphous character in the CS region facilitates e^--h^+ separation. Conversely, to increase mobilities and thus electron and hole transport away from the CS region, the transport regions should carry a high degree of molecular order. Hence, for a heterojunction PV device composed of planar π stacking molecules as CuPc and PTCDA, this study suggests the molecular packing gradually to become more ordered as the electrode regions are approached, as schematically shown in Figure 10.

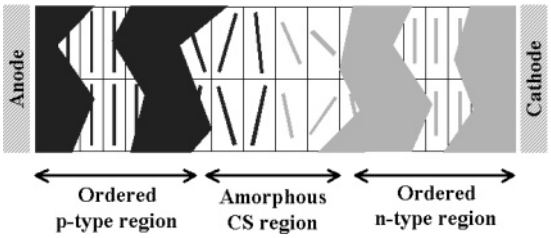

Figure 10. Schematic representation of the idealized structure for a CuPc|PTCDA heterojunction PV device as suggested by this study. Charge separation of short e^--h^+ pairs at the DA interface is facilitated by orientational disorder as opposed to the subsequent transport of carriers in the n- and p-type transport regions, which is facilitated by close packing into molecular π stacks.

Acknowledgment. Carlsbergfondet and the Danish Technical Research Council are acknowledged for financial support and the Danish Center for Scientific Computing (DCSC) is acknowledged for providing computational resources. The author thanks K. Kilså Jensen and A. Komolov for fruitful discussions during the preparation of the manuscript.

References and Notes

(1) Tang, C. W. *Appl. Phys. Lett.* **1986**, *43*, 183.
(2) Peumans, P.; Yakimow, A.; Forrest, S. R. *J. Appl. Phys.* **2003**, *93*, 3693.
(3) Forrest, S. R.; Leu, L. Y.; So, F. F.; Yoon, W. Y. *J.Appl. Phys.* **1989**, *66*, 5908.
(4) Hoppe, H.; Sariciftci, N. S. *J. Mater. Res.* **2004**, *19*, 1924.
(5) Forrest, S. R. *Chem. Rev.* **1997**, *97*, 1793.
(6) Devaux, P.; Quedec, P. *Phys. Lett. A* **1969**, *28*, 537.
(7) Danziger, J.; Dodelet, J.-P.; Lee, P.; Nebesny, K. W.; Armstrong, N. R. *Chem. Mater.* **1991**, *3*, 821.
(8) Al-Mohamad, A.; Soukieh, M. *Thin Solid Films* **1995**, *271*, 132.
(9) Triyana, K.; Yasuda, T.; Fujita, K.; Tsutsui, T. *Thin Solid Films* **2005**, *477*, 198.
(10) Al-Mohamad, A. *Energy Convers. Manage.* **2004**, *45*, 2661.
(11) Rostalski, J.; Meissner, D. *Solar Energy Mater. Solar Cells* **2000**, *63*, 37.
(12) Sylvester-Hvid, K. O.; Rettrup, S.; Ratner, M. A. *J. Phys. Chem. B* **2004**, *108*, 4296.
(13) Sylvester-Hvid, K. O.; Ratner, M. A. *J. Phys. Chem. B* **2005**, *109*, 200.
(14) Hill, I. G.; Kahn, A.; Soos, Z. G.; Pascal, R. A., Jr. *Chem. Phys. Lett.* **2000**, *327*, 181.
(15) Shen, Z.; Forrest, S. R. *Phys. Rev. B* **1997**, *55*, 10578.
(16) Cox, J. J.; Jones, T. S. *Surf. Sci.* **2000**, *457*, 311.
(17) Lemaur, V.; Steel, M.; Beljonne, D.; Brédas, J.-L.; Cornil, J. *J. Am. Chem. Soc.* **2005**, *127*, 6077.
(18) Grätzel, M.; Moser, J.-E. In *Electron Transfer in Chemistry*; Balzani, V., Ed.; Wiley-VCN: New York and Weinheim, 2001; Vol. 5, p 589.
(19) Persson, N.-K.; Ingañas, O. In *Organic Photovoltaics*: *Mechanisms, Materials and Devices*; Sun, S.-S., Sariciftci, N. S., Ed.; CRC Press: Boca Raton, Fl, 2005; Vol. 99, p 107.
(20) Xiao, K. Liu, Y.; Yu, G.; Zhu, D. *Appl. Phys. A* **2003**, *77*, 367.
(21) Gould, R. D. *Thin Solid Films* **1984**, *125*, 63.
(22) Hung, L. S.; Mason, M. G. *Appl. Phys. Lett.* **2001**, *78*, 3732.
(23) Delacote, G.; Fillard, J. F.; Schott, M. *Solid State Commun.* **1966**, *4*, 137.
(24) Delacote, G.; Fillard, J. F.; Marco, F. J. *Solid State Commun.* **1964**, *2*, 373.
(25) Bulović, V.; Forrest, S. R. *Chem. Phys.* **1996**, *210*, 13.
(26) Forrest, S. R.; Burrows, P. E.; Haskal, E. I.; So, F. F. *Phys. Rev. B* **1993**, *49*, 11309.

(27) Ostrick, J. R.; Dodabalapur, A.; Torsi, L.; Lovinger, A. J.; Kwock, E. W.; Miller, T. M.; Galvin, M.; Berggren, M.; Katz, H. E. *J. Appl. Phys.* **1997**, *81*, 6804.

(28) Simon, J.; Andre, J.-J. Molecular Semiconductors—Photoelectrical Properties and Solar Cells; Springer-Verlag: Berlin, 1985.

(29) Ponce, A.; Grey, H. B.; Winkler, J. R. *J. Am. Chem. Soc.* **2000**, *122*, 8187.

(30) Ikushima, A. J.; Kanno, T.; Yoshida, S.; Maeda, A. *Thin Solid Films* **1996**, *273*, 35.

(31) Hill, I. G.; Milliron, D.; Schwartz, J.; Kahn, A. *Appl. Surf. Sci.* **2000**, *166*, 354.

(32) Chassé, T.; Wu, C.-I.; Hill, I. G.; Kahn, A. *J. Appl. Phys.* **1999**, *85*, 6589.

(33) Wu, C. I.; Hirose, Y.; Sirringhaus, H.; Kahn, A. *Chem. Phys. Lett.* **1997**, *272*, 43.

(34) Yoshida, H.; Tokura, Y.; Koda, T. *Chem. Phys.* **1986**, *109*, 375.

(35) Soos, Z. G.; Hennessy, M. H.; Wen, G. *Chem. Phys.* **1998**, *227*, 19.

(36) Bulović, V.; Burrows, P. E.; Forrest, S. R.; Cronin, J. A.; Thompson, M. E. *Chem. Phys.* **1996**, *210*, 1.

(37) Peumans, P.; Forrest, S. R. *Chem. Phys. Lett.* **2004**, *398*, 27.

(38) Lee, Y.-L.; Tsai, W.-C.; Maa, J.-R. *Appl. Surf. Sci.* **2001**, *173*, 352.

(39) Leonhardt, M.; Mager, O.; Port, H. *Chem. Phys. Lett.* **1999**, *313*, 24.

(40) The p- and n-type nomenclature may be ambiguous for compounds such as CuPc and PTCDA due to their ambipolar nature. Here the distinction refers to the preference for hole and electron transport for a specific PV device, and it will be shown later that CuPc appears p-type and PTCDA n-type.

(41) HOMO and LUMO are here taken as properties pertaining to the individual molecules.

(42) For excitons migrating in the D phase, this would involve the transitions $\cdots D^*-D\cdots \rightarrow \cdots D^+-D^-\cdots \rightarrow \cdots D-D^*\cdots$.

(43) Values of γ reported in the literature typically vary from 2 to 15 nm^{-1} depending on the nature of the DA system. As ET is not bridge assisted here, and to ensure not to underestimate the effect of changing the intermolecular distances, a rather strong distance dependence of 10 nm^{-1} is chosen as default.

(44) Note that the LUMO is not taken equal to the electron affinity as frequently done in solid-state physics. The LUMO is a molecular property and promoting an electron from the HOMO to the LUMO costs E_{opt} and here approximates the energy of the Frenkel exciton.

(45) For large mobilities it should be noted that $I_{sc}(d)$ increases on adding the first few monolayers of CuPc. This does not appear on the scale employed in Figure 5 however.

(46) In relating an increase in ϕ to an increase in α and a decrease in β, the geometrical assumption is made that the distance between the edge of a molecule and the closet corners of its corresponding grid cell must remain constant as ϕ changes.

(47) As well as the $\cdots D^+-D-A^-\cdots$ and $\cdots D^+-D-D\text{-}A^-\cdots$ configurations.

(48) The rate for exciton dissociation however still obeys eq 2.